

Electronic absorption spectroscopy of matrix-isolated polycyclic aromatic hydrocarbon cations. I. The naphthalene cation ($C_{10}H_8^+$)

F. Salama and L. J. Allamandola

NASA-Ames Research Center, Space Science Division MS: 245-6, Moffett Field, California 94035

(Received 4 December 1990; accepted 19 February 1991)

The ultraviolet, visible, and near infrared absorption spectra of naphthalene ($C_{10}H_8$) and its radical ion ($C_{10}H_8^+$), formed by vacuum ultraviolet irradiation, were measured in argon and neon matrices at 4.2 K. The associated vibronic band systems and their spectroscopic assignments are discussed together with the physical and chemical conditions governing ion production in the solid phase. The absorption coefficients were calculated for the ion and found lower than previous values, presumably due to the low polarizability of the neon matrix. This study presents the first spectroscopic data for naphthalene trapped in a neon matrix, where the perturbation of the isolated species by its environment is minimum; a condition crucial to astrophysical applications.

I. INTRODUCTION

The experimental results described here for the naphthalene molecular ion ($C_{10}H_8^+$) represent the first in a series of studies on polycyclic aromatic hydrocarbon (PAH) cations isolated in neon matrices. This study of the ultraviolet, visible and near infrared (IR) spectroscopic characteristics of neutral and ionized PAHs isolated in Ne matrices was undertaken because of the recent recognition of their importance in interstellar astrophysics as the missing link between small carbon clusters and amorphous carbon particles. PAHs, which appear to be the most abundant free interstellar organic molecules known ($\sim 17\%$ of the cosmic carbon), are currently considered the best candidates to explain the mid-infrared spectral features emitted from many objects in the interstellar medium.^{1,2} PAHs have also been considered as possible carriers of the well-known visible, diffuse interstellar absorption bands (DIBs) which extend from 4400 Å into the near IR and are characteristic of an important, ubiquitous component of interstellar space.³ While the PAHs have been postulated as an important interstellar constituent, the ultraviolet-visible-near infrared absorption properties of the *free species*, necessary to understand the radiation and energy balance in space, are not known. The main hypothesis in the model dealing with the interstellar spectral features is that PAHs—present as a mixture of radicals and positive ions as well as neutral species (perhaps partially (30%) hydrogenated)—are responsible for most of the infrared emission bands which are associated with UV-rich regions of planetary and reflection nebula, HII regions, stellar objects, and extragalactic sources. It is the purpose of these studies to obtain quantitative ultraviolet-visible-near infrared spectroscopic data on isolated, neutral and ionized PAHs.

The matrix isolation technique^{4,5} provides a powerful tool, not only to simulate the low temperature (4–15 K) and isolated conditions in space, but also because it is particularly well suited to the study of such large, nonvolatile, reactive molecules. Among the rare gases commonly used as matrix-cage material (Ne, Ar, Kr, and Xe), solid neon provides the

best (i.e., less polarizable) medium for the study of quasi-unperturbed ionic spectra.⁶

The naphthalene cation has been studied in detail in the ultraviolet-to-near infrared range by absorption spectroscopy in glassy organic solids,⁷ in solution,⁸ and in argon and krypton matrices.⁹ Gas-phase data have been provided by the multiphoton dissociation spectra of $C_{10}H_8^+$ ¹⁰ and the photoelectron spectra (PES) of naphthalene.¹¹ The vibrational spectrum of the ground-state naphthalene cation has been measured by resonant Raman spectroscopy¹² in a glassy solid. Naphthalene cations were formed, here, by direct photoionization of the matrix-isolated neutral precursor ($C_{10}H_8$) and vibronic absorption spectra were recorded from 180 nm ($55\,500\text{ cm}^{-1}$) to 900 nm ($11\,100\text{ cm}^{-1}$). The ultraviolet-visible spectrophotometer coupled with a low temperature (4.2 K) sample chamber, developed for this study, is described in Sec. II. The following Sec. III, presents the absorption spectra of neutral naphthalene and its cation, together with a discussion of the role the various experimental parameters play in the measurements. The discussion of the results and the spectroscopic assignments are reported in Sec. IV and the conclusions of the study are given in Sec. V.

II. EXPERIMENTAL

A computer-controlled UV-visible spectrophotometer system, coupled to a helium-cooled cryogenic cell, was designed and developed to measure the absorption and emission spectra of neutral, ionic, or radical species of interstellar and planetary interest using matrix isolation spectroscopic techniques. A description of the apparatus, represented schematically in Fig. 1, is given in this section. It consists of the following parts:

(i) The Spectral Light Source (LS): The visible light source is a Quartz Tungsten Halogen lamp (Ushio FCR) which provides a bright and stable output from 320 to 2500 nm when equipped with a stabilized DC power supply (Oriel 68735). The UV source is a deuterium lamp (Hamamatsu L 1626) equipped with a current regulated power supply (Ha-

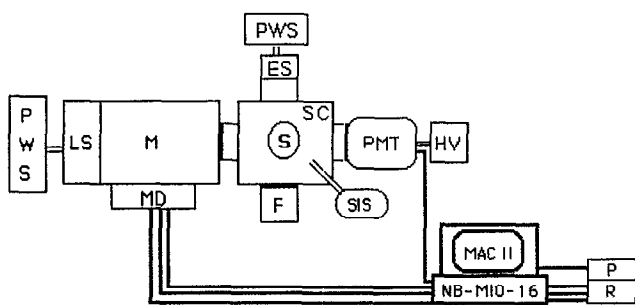


FIG. 1. Block diagram of computer controlled ultraviolet-visible spectrophotometer. (ES): Vacuum ultraviolet excitation source; (F): vacuum furnace; (HV): high voltage power supply for detector; (LS): spectral light source; (M): scanning monochromator; (MAC): microcomputer; (MD): monochromator drive; (NB-MIO): multiple input output NuBus board; (P) printer; (PMT): photomultiplier tube; (PWS): power supplies; (R): strip chart recorder; (S): sample substrate; (SC): cryogenic sample vacuum chamber; (SIS): sample introduction system.

mamatsu C 1518). It provides a smooth continuum from 160 to 360 nm with a low visible and infrared output.

(ii) The Monochromator (M): The monochromator has a symmetrical Czerny-Turner optics configuration (Photon Technology International 01-002) which can accommodate two fixed gratings on a rotatable mount. The focal length is 200 mm and the aperture ratio is $f/4$. The two ruled gratings used (1200 line/mm) are blazed at 250 and 500 nm with absolute peak efficiencies of 60% in the UV and 70% in the visible. The linear dispersion is 4 nm/mm over the entire wavelength range (180–900 nm). The monochromator is equipped with micrometer adjustable entrance and exit slits (0–6.5 mm \times 10–20 mm) providing a resolution of 1 nm at 0.25 mm slit width. An external stepping motor (16 steps/nm) and a home-built controller programmed via a microcomputer (APPLE MACINTOSH II) through a NuBus board (National Instrument NB-MIO-16) are used to drive the monochromator (12–480 nm/min). Wavelength calibration and testing of the resolution of the monochromator are performed with spectral line lamps (Oriel, Spectral calibration set 6053). In the absorption configuration, the light source(s) and the monochromator are mounted on a single optical bench to optimize the stability of the optical alignment.

(iii) The Cryogenic Sample Chamber (SC): The sample chamber is part of a stainless-steel, ultra-high vacuum system and contains four ports at 90° and two gas injection ports at 45° angles. The cryogenic sample holder, suspended in the center of the chamber at the tip of the cooler, is designed to accommodate a 20 \times 1 mm sapphire window (S). An ultra-high vacuum ($P < 2.0 \times 10^{-8}$ T) is maintained at all times with a standard set of diffusion (Edwards Diffstack MK2) and mechanical rotary (Edwards E2M5) pumps protected from contamination by a liquid nitrogen cold trap and a fore-line activated alumina trap. The pressure is continuously monitored with ion (CVC GIC-048-2) and thermocouple gauges (CVC GTC-036) mounted on the manifold. The substrate is cooled down to 4.2 K by a variable temperature-liquid helium transfer cryostat (High Tran Refrigerator,

Hansen Associates HLT-183). The temperature of the substrate is controlled automatically from the lowest limit (4.2 K) to room temperature by a resistive heater operated by a programmable controller (Hansen Associates Series 8000) used in conjunction with regulating the liquid helium flow through a needle valve mounted at the end of the transfer line or by adjusting the exhaust gas back pressure on the High Tran exhaust port. The temperature of the substrate is measured with an Fe–Au/Chromel thermocouple connected to the sample holder. A second and similar sensor attached to the cold head of the cryocooler provides a measure of the temperature gradient between the sample and the refrigerator. The substrate can be rotated through 360° without breaking the vacuum and can be positioned to face alternatively the spectroscopy ports equipped with fused-silica windows (Rolyn Optics), the gas injection ports, an excitation lamp, or vacuum deposition furnace.

(iv) The Photo Excitation Source (ES): The vacuum ultraviolet radiation used to photolyze the sample is generated by a microwave-powered, flowing hydrogen, discharge lamp. The lamp consists of a tunable McCarroll cavity (Ophos Instruments) mounted onto a glass discharge tube and powered by a 50–120 W microwave generator (Ophos Instruments MPG 4M). The lamp, equipped with a removable MgF₂ window, is mounted on one of the ports of the sample chamber. The microwave discharge in pure hydrogen generates a 20 nm-wide band centered around 160 nm as well as atomic resonance lines including strong Lyman α emission at 121.6 nm.¹³ When operating with pure H₂ at a pressure of 1 to 2 T, the flux is $\sim 2 \times 10^{15}$ photons cm⁻² s⁻¹ equally distributed between the 160 nm band and the Lyman α line. By using a 10% hydrogen/helium mixture in a low pressure discharge, one can get most of this flux as nearly monochromatic radiation in the Lyman α line.^{13(b),(c)}

(v) The Photon Detector (PMT): The detector module is comprised of a photomultiplier tube (Hamamatsu R955) sensitive in the spectral range from the ultraviolet to the near infrared (160–900 nm, peaking at 400 nm) and mounted directly on one of the spectroscopy ports of the sample chamber. The PMT is biased by a negative high voltage of 800 volt provided by a regulated DC power supply (Power Designs Pacific HV-1544) to ensure a linear response with a low dark current ($\leq 0.5\%$). The analog output signal is transmitted to the microcomputer interfaced to the spectrometer through a NuBus board for digitization, analysis and display and is plotted on a strip chart recorder (Kipp & Zonen BD 41).

The entire system is monitored and controlled with a microcomputer (APPLE MACINTOSH II) through a multiple input output data acquisition board (National Instruments NB-MIO-16H) which processes the detector signal and provides timing signals to the step motor driver for use in controlling the monochromator. The hardware is controlled through a home-made program¹⁴ developed using the graphical programming language (G) of the Laboratory Virtual Instrument Engineering Workbench software (LabVIEW, National Instruments), a set of device drivers for the NuBus board, and built-in functions provided in the accompanying LabDriver Library. The first program, called “UV–

Visible Spectrometer”, allows the user to operate the system in the single-beam mode and to automate the data acquisition process after selecting the instrumental parameters. A second program, called “UV–Visible Spectrophotometer”, calculates the transmittance [$T = I/I_0$, where I_0 and I are associated with the scans before and after deposition of the sample on the cold window, respectively, or to the scans of the sample before and after vacuum ultraviolet (VUV) irradiation] and/or absorbance [$-\log_{10}(T)$] spectra from the ratio of the single beam spectra data point previously recorded. In the case of emission spectroscopy, the resulting spectrum can either be a single beam spectrum or the difference of two single beam spectra. The “UV–Visible Spectrophotometer” program also performs a base line correction and calculates the integrated surface area associated with each of the spectral features selected through the peak picking routine. Absorbance, transmittance, and/or emission spectra are plotted as a function of wavelength in a strip chart panel associated with the program and can eventually be sent to a printer.

III. RESULTS

Each experiment described here consisted of the following protocol: recording of the single-beam absorption spectrum of the cold blank substrate (I_{blank}), condensation of the argon or neon matrix on the cold window at 4.2 K, measurement of the single-beam absorption spectrum of the matrix-isolated neutral precursor (I_{neutral}), exposure of the sample to VUV irradiation for a given time, t , and, finally, recording of the single-beam absorption spectrum of the irradiated sample (I_{irrad}). The last two steps were repeated at different intervals to monitor the dependence of the new spectral features produced on VUV photolysis. The effects of parameters such as: matrix material M , duration of VUV irradiation, concentration of the reactant R in the matrix material M , photon energy of the excitation source in the VUV (i.e., the flux of the Lyman α line with respect to the 160 nm band), photolysis simultaneous with deposition vs *in situ* photolysis, matrix temperature (in the case of Ar matrices), and the presence of an electron scavenger (acceptor) in the matrix were investigated to optimize the number of ions formed and stabilized in the matrix under VUV excitation. All spectra were recorded over the entire range (180–900 nm) of the spectrophotometer system. All of the samples were prepared by premixing naphthalene vapor with the rare gas (Ar or Ne) at room temperature. Naphthalene has a vapor pressure of about 0.15 T when in equilibrium with the solid at room temperature.¹⁵ The spectroscopic results described in this section were generally obtained under the following standard experimental conditions (unless specified otherwise): $R:M = 1:600$; substrate temperature: 4.2 K; sample deposition rate: 10 mmole h^{-1} for 2 h; monochromatic VUV irradiation in the Lyman α line (121.6 nm). Naphthalene crystals (Aldrich 99%) were further purified by several trap to trap distillations prior to use while Ar (Matheson 99.9995%) and Ne (Cryogenic Rare Gas 99.999%) research grade rare gases were used without further purification.

A. Naphthalene

1. Spectroscopy

The absorption spectrum of naphthalene embedded in an Ar or Ne matrix can be divided into three distinct band systems with very different intensities [see Figs. 2(a) and 2(b)]. The longest wavelength system, or System I, is very weak, with a gas-phase oscillator strength of about 0.002.¹⁶ The strongest band of this system falls at 309.2 ± 0.1 nm in Ar and 307.6 ± 0.1 nm in Ne. System II peaks near 272.5 ± 0.1 nm in Ar (268.5 ± 0.3 nm in Ne) and is moderately strong, with a gas-phase oscillator strength on the order of 0.1.¹⁶ System III is very strong (gas-phase oscillator strength on the order of 1.0)¹⁶ with the strongest band at 216.2 ± 0.3 nm in Ar and 211.6 ± 0.3 nm in Ne. The measurements are limited on the short wavelength side ($\lambda < 200$ nm) by overlap with the strong Schumann–Runge system of atmospheric O_2 ($B^3\Sigma_u^- \leftarrow X^3\Sigma_g^-$ transition).¹⁷ The vibronic band wavelengths, frequencies, intervals, and assignments are listed in Table I for Ne and Ar matrices. The Ne-to-Ar relative shifts in the energy of the excited vibronic levels ($\Delta\nu/\nu_{\text{Ne}}$) are also reported in the last column of the table. The vibronic spacings listed are broken down into possible fundamental modes. These fundamentals and their assignments are summarized in Table II (see Sec. IV A). The data indicate a red shift in energy for all the levels when going from a neon to an argon matrix as expected from the fourfold increase in the polarizability of the matrix material.¹⁸ This shift is proportional to the energy of the transition and increases from a mean value of about 0.5% for System I, to 1.5% for System II, and 2.0% for System III indicating that the interaction between the naphthalene molecule and the rare gas atoms of the lattice increases as higher excited molecular electronic states are reached. On the other hand, comparison of our measurements with spectra of naphthalene in the gas phase¹⁹ shows that the gas phase to neon relative matrix shift ($\Delta\nu/\nu_{\text{Gas}}$) is much smaller, averaging 0.25% for the strongest band of each of all the three absorption systems. The wide range in oscillator strengths of these three systems required distinct experimental conditions to optimize the spectrum of each particular system. These conditions were: a very thin matrix (5 min deposit at a rate of 10 mmole h^{-1}) for System III; a moderately thick matrix (30 min deposit at a rate of 10 mmole h^{-1}) for System II, and a thick matrix (2 h deposit at a rate of 10 mmole h^{-1}) for System I, respectively.

B. Naphthalene cation

1. Spectroscopy

VUV irradiation of the sample (121.6 nm line) for as short as 60 s, produces new spectral features in the 220–680 nm range in both matrices (Figs. 3 and 4). Seven new band systems are detected in neon matrices and five in argon. The new absorption bands, together with their assignments, frequencies, and frequency intervals, are summarized in Table III. The strongest peak in the visible system falls at 675.0 ± 0.3 nm [72 cm^{-1} full width at half maximum (FWHM)] in Ar and 674.1 ± 0.3 nm (120 cm^{-1} FWHM)

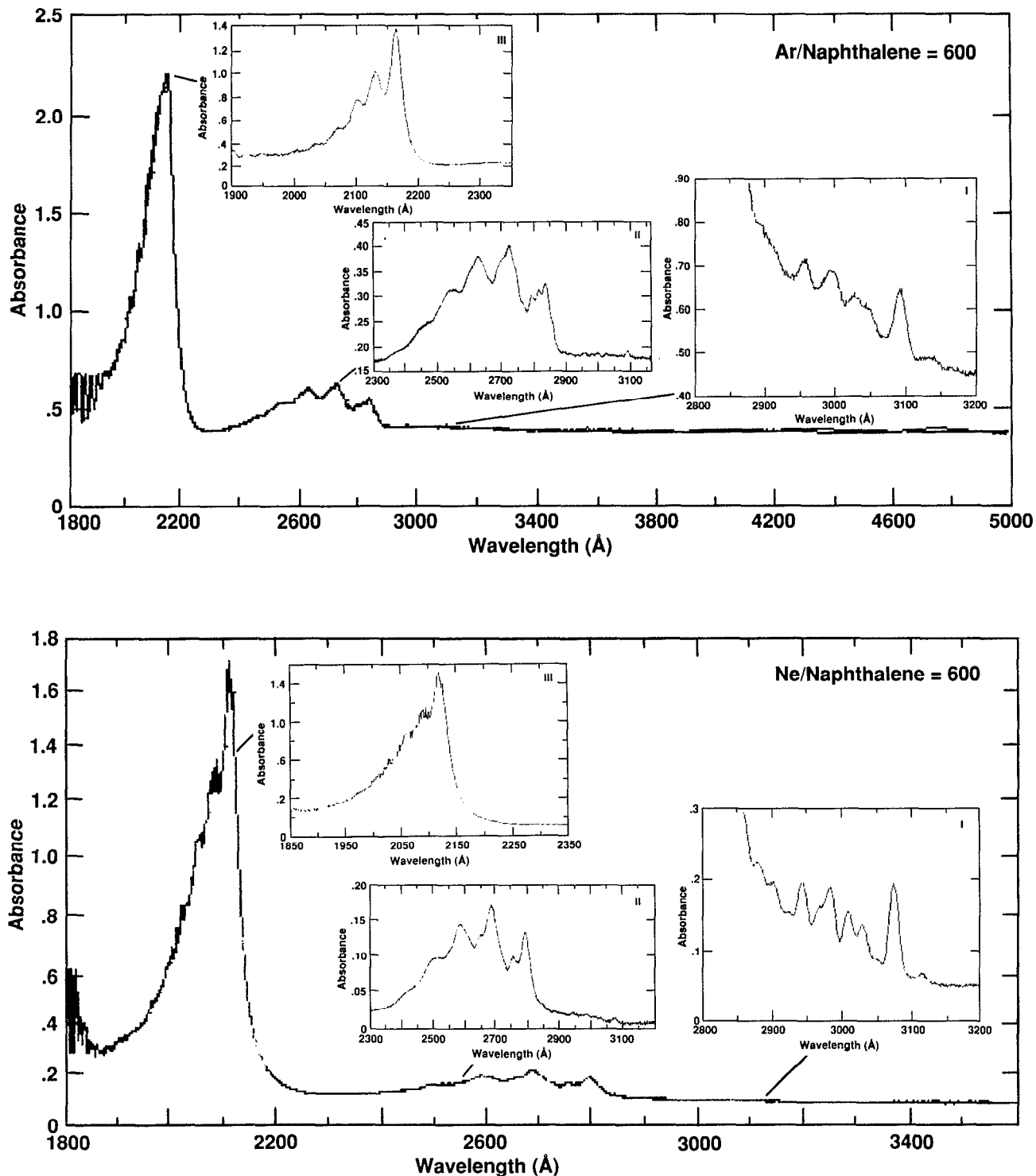


FIG. 2. The absorption spectrum of matrix isolated naphthalene ($M/R = 600$, deposition rate = 10 mmole h^{-1} , $T = 4.2 \text{ K}$). Argon matrix, full spectrum corresponds to 35 minute deposition. Inserts I, II, and III correspond to 120, 35, and 15 minute deposition, respectively. Neon matrix: full spectrum corresponds to 10 minute deposition. Inserts I, II, and III correspond to 120, 20, and 10 minute, respectively.

in Ne. Of the six other systems most are blended with Systems I, II, and III of neutral naphthalene. These bands, although difficult to measure, are correlated with the visible bands. In a Ne matrix, the strongest components peak at $456 \pm 0.4 \text{ nm}$, $376.9 \pm 0.5 \text{ nm}$, $305.0 \pm 0.2 \text{ nm}$, $276.0 \pm 1.0 \text{ nm}$, $244.3 \pm 0.8 \text{ nm}$, and $222.7 \text{ nm} \pm 1.0 \text{ nm}$. In an Ar matrix, only four of the six systems are discernable with the

corresponding absorptions peaking at $379.8 \pm 0.1 \text{ nm}$, $307.8 \pm 0.1 \text{ nm}$, $274.5 \pm 1.0 \text{ nm}$, and $219.1 \pm 1.0 \text{ nm}$, respectively. A faint visible luminescence was observed from the irradiated samples as they were warmed from 30 to 50 K and the molecular ions (anions and cations) allowed to diffuse in the argon matrix.

We attribute all of these new features produced by VUV

TABLE I. Vibronic transitions of neutral naphthalene isolated in neon and argon matrices. The number in parentheses indicates the value of σ^2 ; * represents a single measurement with a 1.0 nm uncertainty.

Ne				Ar				Rel. Shift
λ (nm)	ν (cm ⁻¹)	$\Delta\nu$ (cm ⁻¹)	Assignment ^a	λ (nm)	ν (cm ⁻¹)	$\Delta\nu$ (cm ⁻¹)	Assignment ^a	$\Delta\nu_{(\text{Ne-Ar})}/\nu_{\text{Ne}}$ (%)
[System IV: ¹A_g(S₄) ← X¹A_g(S₀)]^b								
...	200.7*	49 826	1563 (877 + 710)	[2ν ₈ (b _{1g}) + ν ₈ (a _g)]	...
201.9*	49 530	438	ν ₈ (b _{1g})	203.5*	49 140	877	2ν ₈ (b _{1g})	0.8
203.7*	49 092	0	...	207.2*	48 263	0	...	1.7
System III: ¹B_{3u}(S₃) ← X¹A_g(S₀)								
205.7*	48 615	1356	ν ₄ (b _{1g})	210.1(0.3)	47 604	1344	ν ₄ (b _{1g})	2.1
208.9*	47 870	611	...	212.9(0.2)	46 970	710	ν ₈ (a _g)	1.9
211.6(0.3) ^c	47 259	0	...	216.2(0.3) ^c	46 260	0	...	2.1
System II: ¹B_{2u}(S₂) ← X¹A_g(S₀)								
242.3(0.4)	41 278	5463	...	248.1*	40 306	5045	...	2.4
250.3(0.9)	39 953	4138	...	255.7(0.1)	39 116	3855	...	2.1
258.3(0.5)	38 708	2893	2ν ₄ (a _g)	262.7(0.1)	38 061	2800	2ν ₄ (a _g)	1.7
265.5*	37 665	1850	[ν ₄ (a _g) + ν ₈ (b _{1g})];
			2ν ₇ (b _{1g});					
			2[ν ₈ (b _{1g}) + ν ₉ (a _g)]					
268.5(0.3) ^c	37 249	1434	ν ₄ (a _g);	272.5(0.1) ^c	36 697	1436	ν ₄ (a _g);	1.5
			[ν ₉ (a _g) + ν ₇ (b _{1g})];				[ν ₉ (a _g) + ν ₇ (b _{1g})];	
			[2ν ₉ (a _g) + ν ₈ (b _{1g})]				[2ν ₉ (a _g) + ν ₈ (b _{1g})]	
275.4(0.3)	36 314	499	ν ₉ (a _g)	279.2(0.3)	35 817	556	ν ₉ (a _g)	1.4
...	281.8(0.2)	35 486	225
279.2(0.3)	35 815	0	...	283.6(0.2)	35 261	0	...	1.5
System I: ¹B_{3u}(S₁) ← X¹A_g(S₀)								
288.0(0.1)	34 726	2624
290.0(0.1)	34 490	2388	[ν ₇ (b _{1g}) (1422 + 914) (1422 + 1000)]
			+ ν ₄ (a _g);					
			[ν ₄ (a _g) + 2ν ₉ (a _g)]					
294.3(0.2)	33 980	1878	[ν ₄ (a _g) (1422 + 413) (2 × 914)]	295.8(0.1)	33 807	1960 (1531 + 413)	3ν ₈ (b _{1g}) + ν ₈ (a _g)	0.5
			2ν ₇ (b _{1g});					
			2[ν ₈ (b _{1g}) + ν ₉ (a _g)]					
297.3*	33 636	1534	2ν ₈ (b _{1g})
			(1125 + 413) + ν ₈ (a _g)					
298.3(0.3)	33 524	1422	ν ₄ (a _g);	299.6*	33 378	1531 (1118 + 413)	2ν ₈ (b _{1g}) + ν ₈ (a _g)	0.4
			[ν ₉ (a _g) + ν ₇ (b _{1g})];					
			[2ν ₉ (a _g) + ν ₈ (b _{1g})];					
			2ν ₈ (a _g)					
301.0(0.1)	33 227	1125 (413 + 710)	ν ₈ (b _{1g}) + ν ₈ (a _g)	302.8(0.1)	33 031	1184 (500 + 710)	[ν ₉ (a _g) + ν ₈ (a _g)];	0.6
							ν ₅ (b _{1g})	
302.9(0.3)	33 016	914	ν ₇ (b _{1g});	303.4(1.0)	32 965	1118 (413 + 710)	ν ₈ (b _{1g}) + ν ₈ (a _g)	0.6
			[ν ₈ (b _{1g}) + ν ₉ (a _g)]					
307.6(0.1) ^c	32 515	413	ν ₈ (b _{1g})	309.2(0.1) ^c	32 347	500	ν ₉ (a _g)	0.5
311.5(0.2)	32 102	0	...	314.0*	31 847	0	...	0.8

^a Assignment based on high resolution measurements of Refs. 19(a) and 30(b).^b Assigned following Ref. 30(a). (See text.)^c Strongest band of the system.

TABLE II. Comparison of the repeating vibrational frequencies (in cm^{-1}) for matrix-isolated neutral naphthalene in the S_1 , S_2 , S_3 and S_4 electronic excited states with the S_1 state gas phase data.

Vibrational mode ^a	Gas ^b	Ne ^c	Ar ^c
$\nu_8(b_{1g})$	435(S_1)	413(S_1) 438(S_4)	413(S_1) 438(S_4)
$\nu_9(a_g)$	501(S_1)	...	500(S_1)
$\nu_8(a_g)$	700(S_1)	499(S_2) 710(S_1)	556(S_2) 710(S_1) 710(S_3)
$\nu_7(b_{1g})$	910(S_1)	914(S_1)	...
$\nu_5(b_{1g})$	1196(S_1)	...	1184(S_1)
$\nu_4(b_{1g})$	1376(S_1)	1356(S_3)	1344(S_3)
$\nu_4(a_g)$	1432(S_1)	1422(S_1) 1434(S_2)	... 1436(S_2)

^a Following the conventional nomenclature (Ref. 37), the vibrations of a specific symmetry are numbered, "1" being the normal mode of highest frequency. The symmetry indicated for each vibration is related to the molecular configuration defined in the text.

^b Reference 19(a).

^c This work.

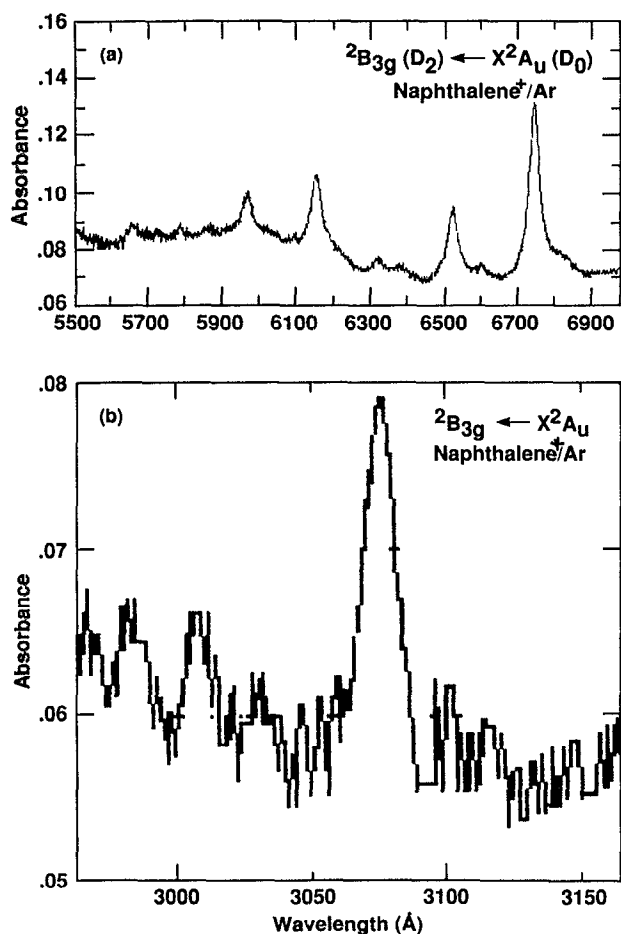


FIG. 3. The absorption spectrum of the naphthalene cation isolated in an argon matrix (Naphthalene/Argon = 1/600, VUV irradiation time = 10 min, $T = 4.2$ K). The deposition time is 120 min for (a) and 35 min for (b) at a rate of 10 mmole h^{-1} .

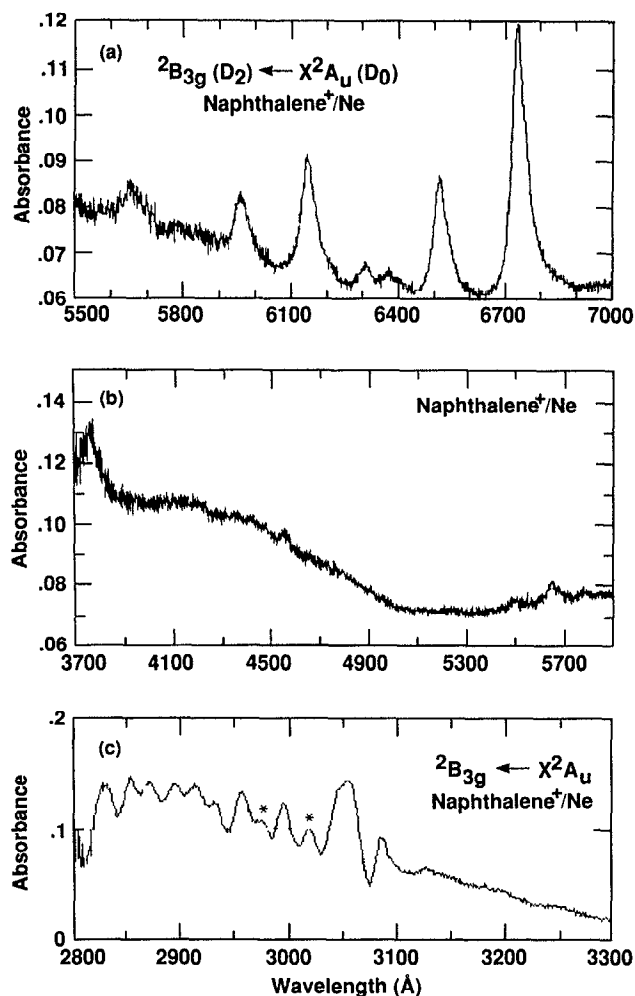


FIG. 4. The absorption spectrum of the naphthalene cation isolated in a neon matrix (Naphthalene/Neon = 1/600, deposition rate = 10 mmole h^{-1} , $T = 4.2$ K). (a) 150 min deposit, 75 min VUV; (b) 150 min deposit, 60 min VUV; (c) 120 min deposit, 90 min VUV. (*) absorption bands of the remaining neutral naphthalene.

irradiation to the naphthalene cation ($C_{10}H_8^+$) on the basis of their similarities in position, relative intensities, and general behavior under irradiation and warm up to those previously assigned to this ion and measured with different cation formation techniques.⁷⁻¹¹ The lowest energy absorption system origin measured at 674.1 nm in Ne matrices (675.0 nm in Ar) is close to the peak position of the band system associated with $C_{10}H_8^+$ in γ -irradiated glasses at 77 K; e.g., 700 nm in organic matrices^{7(a),(c)} and 690 nm in a Freon glass.^{7(b)} Moreover, this value matches the 675.2 nm band of Ar-matrix isolated $C_{10}H_8^+$ formed by photoionization of neutral naphthalene $C_{10}H_8$ ^{9(a),(b),(c)} or by electron impact techniques.^{9(d)} Similar agreement to within 10 Å is found when comparing the other band system origins listed in Table III with the values of 465, 385, and 310 nm in Freon glasses^{7(b)} and 461, 381, 308, and 275 nm in Ar matrices.^{9(b)}

Our results in both matrices (Ar and Ne) also show a very good correlation with the measured photoelectron spectra (PES) of gas phase naphthalene.^{11(a),(b),(c),(d)} The comparison between the gas phase PES band differences

TABLE III. Vibronic transitions of naphthalene cation isolated in neon and argon matrices. The number in parentheses indicates the value of σ^2 .

Ne			Ar			$\Delta(\text{Ne-Ar})$
$\lambda(\text{nm})$	$\nu(\text{cm}^{-1})$	$\Delta\nu(\text{cm}^{-1})$	$\lambda(\text{nm})$	$\nu(\text{cm}^{-1})$	$\Delta\nu(\text{cm}^{-1})$	$\Delta\nu(\text{cm}^{-1})$
222.7 ^a	44 903	0	² B _{2g} ← X ² A _u (D ₀)			- 738
			219.1 ^a	45 641	0	
244.3(0.8)	40 933	0	² T _{1g} ← X ² A _u (D ₀)			...
...
...	² B _{3g} ← X ² A _u (D ₀)			...
...	257.3 ^a	38 865	2435	...
...	265.4 ^a	37 679	1249	...
...	267.0 ^a	37 453	1023	...
274.2(0.3)	36 470	238 (site)
276.0 ^{a,b}	36 232	0	274.5 ^{a,b}	36 430	0	198
283.0(0.5)	35 336	2963	² B _{3g} ← X ² A _u (D ₀)			...
285.4 ^a	35 039	2666
287.1 ^a	34 831	2458
289.3 ^a	34 566	2193
291.2(0.2)	34 341	1968
293.1 ^a	34 118	1745
295.9(0.5)	33 795	1422	299.0 ^a	33 445
299.5(0.4)	33 389	1016	301.0 ^a	33 223
305.0(0.2) ^b	32 787	414	307.8(0.1) ^b	32 492	...	295
308.9(0.4)	32 373	0
356.0 ^a	28 090	1558	² B _{2g} (D ₄) ← X ² A _u (D ₀)			...
363.0 ^a	27 548	1016
376.9(0.5) ^b	26 532	0	379.8(0.1)	26 330	0	202
456(0.4)	21 930		² B _{2g} (D ₃) ← X ² A _u (D ₀)			...
511.4(0.4)	19 554	4719	² B _{3g} (D ₂) ← X ² A _u (D ₀)			...
		849 + 2 × (1423 + 502)	510.9(0.3)	19 574	4759	- 20
		(5 × 849 + 502)			849 + 2 × (1423 + 507)	
...	523.8(0.1)	19 091	(5 × 849 + 507)	...
534.1(0.5)	18 723	3888	4276	...
		2 × (1423 + 502)			(3 × 1423)	...
		4 × 849 + 502		
550.3(0.8)	18 172	3337	549.9(0.5)	18 186	3371	- 14
		(502 + 2 × 1423)			(507 + 2 × 1423)	
		(5 × 502 + 849)			(5 × 507 + 849)	
565.8(0.4)	17 674	2839	566.1(0.3)	17 666	2851	8
		(2 × 1423)			(2 × 1423)	
		(4 × 502 + 849)			(4 × 507 + 849)	
...	572.8(0.1)	17 458	2643	...
578.4(0.8)	17 289	2454	579.8(0.5)	17 246	(site)	43
		(1930 + 502)			(1924 + 507)	
		(2 × 502 + 1423)			(2 × 507 + 1423)	
584.8(0.6)	17 100	2265	586.5(1.0)	17 050	2235	50
		(1423 + 849)			(1423 + 849)	
596.5(0.3)	16 765	1930	597.4(0.5)	16 739	1924	26
		(1423 + 502)			(1423 + 507)	
615.1(0.3)	16 258	1423	615.8(0.3)	16 238	1423	20
631.4(0.3)	15 838	1003	632.6(0.3)	15 808	993	30
		(2 × 502)			(2 × 507)	
637.6(0.3)	15 684	849	638.4(0.1)	15 664	849	20
652.0(0.3)	15 337	502	652.7(0.3)	15 322	507	15
...	659.8(0.6)	15 157	(site)	...
674.1(0.3) ^b	14 835	0	675.0(0.3) ^b	14 815	0	20
...	682.8(0.2)	14 646	(site)	...

^a Represents a single measurement with a 1.0 nm uncertainty.^b Strongest band of the system.

$[(I_n - I_1)]$, where I_n is the n^{th} ionization potential with $n > 1$] and our Ne and Ar matrix absorption measurements, reported in Table IV, shows that the reported differences in energy between the first and third PES peaks ($I_3 - I_1$) is in reasonably good agreement with the matrix measurements of $14\,835 \pm 20 \text{ cm}^{-1}$ (674.1 nm) in Ne and $14\,815 \pm 20 \text{ cm}^{-1}$ (675.0 nm) in Ar for the corresponding absorption system origins, respectively. Similarly, the other weak visible absorption progression associated with C₁₀H₈⁺ and observed at $21\,930 \pm 20 \text{ cm}^{-1}$ (456.0 nm) in a Ne matrix is very close to the reported ($I_4 - I_1$) energy differences of the PES data. No further correspondence can be established between the optical and PES spectral features of C₁₀H₈⁺ since the latter measurements can only be compared with the photon-induced absorptions corresponding to transitions from the fully occupied molecular orbitals such as b, c, d, and e and the partially occupied orbital f of Fig. 5.^{10(a),20} Thus, the 11.42 eV PES peak measured by Clark *et al.*^{11(c)} and which appears close to the $26\,532 \text{ cm}^{-1}$ (376.9 nm) absorption band in a Ne matrix ($26\,330 \text{ cm}^{-1}$ (379.8 nm) in an Ar matrix) most probably involves a σ -type excitation originating from levels not represented in Fig. 5 (The σ ionizations are expected to occur above 10 eV in the photoelectron spectra of naphthalene).²¹ The same caution needs to be applied when considering the PES peak at $13.2 \text{ eV}^{11(b),(c)}$ which corresponds to an energy of about $41\,000 \text{ cm}^{-1}$ above the first ionization potential I_1 , a value close to the ultraviolet absorption frequency at $40\,933 \text{ cm}^{-1}$ (244.3

nm) in Ne matrices. Tentative PES peak assignments are also given in Table IV.

In addition, the multiphoton dissociation spectrum of C₁₀H₈⁺^{10(b)} shows two broad bands peaking at about $33\,200$ and $38\,300 \text{ cm}^{-1}$, close to the $32\,373 \text{ cm}^{-1}$ (308.9 nm) and $36\,232 \text{ cm}^{-1}$ (276.0 nm) values measured in Ne matrices while the C₁₀H₈⁺ optical peaks deduced from a previous low-resolution study of the photodissociation spectrum of methylnaphthalene cations^{10(a)} fall close to $15\,000$, $22\,000$, $26\,000$, and $32\,500 \text{ cm}^{-1}$, again in good agreement with the position of the four lower energy absorption band origins in rare gas matrices (see Table III).

Finally, very recent INDO/S-Cl (incomplete neglect of differential overlap/single configuration interaction) calculations by Du and Loew²⁰ show *only seven* optically allowed electronic transitions of the naphthalene cation in the range measured in our experiments [up to $50\,000 \text{ cm}^{-1}$ (200 nm)] and verify the attribution of the seven band systems to the naphthalene cation as listed in Table III. (*Note:* A broad and strong continuum, extending from the ultraviolet to the visible appears to be correlated with the spectrum of the cation. This absorption, which may be very important for astrophysical applications, is not discussed here, but will be considered separately.)

2. Cation production

The effects of various parameters such as naphthalene concentration, duration of exposure to VUV irradiation, the

TABLE IV. Comparison of the naphthalene cation optical transitions with the photoelectron spectra.

	I_1	$I_i - I_1$ (eV)	$I_i - I_1$ (nm)	$I_i - I_1$ (cm ⁻¹)	ν Ne (cm ⁻¹)	Assignment
Eland <i>et al.</i> [Ref. 11(a)]						
	8.12	0		0	This work	
I_1	8.90	0.78	1589.90	6290	...	e-f (optic. forbidden)
I_2	10.00	1.88	659.64	15 160	14 835	d-f
I_3	10.85	2.73	454.26	22 014	21 930	c-f
I_4						
Dewar <i>et al.</i> [Ref. 11(b)]						
	8.11	0		0	This work	
I_1	8.79	0.68	1823.71	5483	...	e-f (optic. forbidden)
I_2	9.96	1.85	670.34	14 918	14 835	d-f
I_3	10.90	2.79	444.49	22 498	21 930	c-f
I_4	12.26	4.15	298.83	33 464	32 373	no correspondence
I_5	13.22	5.11	242.69	41 206	40 933	no correspondence
I_6						
Heilbronner <i>et al.</i> [Ref. 11(d)]						
	8.18	0		0	This work	
I_1	8.86	0.68	1823.71	5483	...	e-f (optic. forbidden)
I_2	10.07	1.89	656.15	15 240	14 835	d-f
I_3						
Clark <i>et al.</i> [Ref. 11(c)] (Adapted from Fig. 1, p. 1416)						
	8.17	0		0	This work	
I_1	8.33	0.16	7750.78	1290		C-C stretch
	8.50	0.33	3757.96	2661		2 × C-C stretch
I_2	8.92	0.75	1653.50	6048	...	e-f (optic. forbidden)
I_3	10.00	1.83	677.66	14 757	14 835	d-f
I_4	10.83	2.66	466.21	21 449	21 930	c-f
	11.00	2.83	438.21	22 820	...	c-f + C-C stretch
I_5	11.42	3.25	381.58	26 207	26 532	No correspondence
I_6	11.83	3.66	338.83	29 513		No correspondence
I_7	12.42	4.25	291.79	34 271	32 373	No correspondence
I_8	13.25	5.08	244.12	40 964	40 933	No correspondence

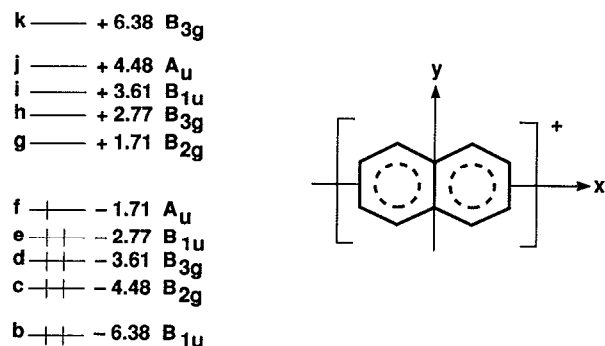


FIG. 5. The Hückel molecular orbital energy levels of the naphthalene cation.

energy of the VUV, sample temperature, the inclusion of an electron acceptor in the matrix, and deposition conditions, were systematically examined in an attempt to optimize the number of naphthalene cations formed and stabilized in the matrix and to provide information on the physico-chemical properties of these molecular ions. In most cases, the tests were performed in Ar matrices. The results are summarized below.

Concentration dependence: The effect of naphthalene concentration in the rare gas matrix (M/R) on the ion yield, shown in Fig. 6, was determined by measuring the cation absorption band strength as a function of concentration, with all other parameters constant. It is clear from the results shown in Fig. 6 that the cation yield depends strongly on the M/R ratio in the range $M/R = 300$ –1000 while it is only slightly changed in the lower concentration range, $M/R = 1000$ –2000. The highest ionic yield is reached with a rare gas matrix to naphthalene ratio of 600. This behavior can be qualitatively understood in terms of two opposing effects: For a constant VUV flux, the total number of ions formed must depend on the number of neutral precursors initially available in the matrix, conversely, the degree of isolation of a neutral precursor in the rare gas cage—i.e., the

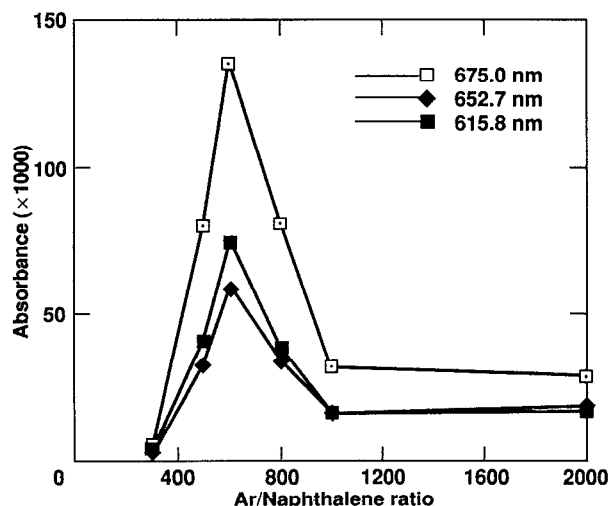


FIG. 6. The concentration dependence of the naphthalene cation.

average separation between two nearest neighbors of the same species—is inversely proportional to the concentration. Statistically, the fraction of isolated naphthalene molecules—or monomers—decreases from 99.5% at $M/R = 2000$ to about 98% at $M/R = 600$ to 96% at $M/R = 300$.²² Electrons can readily propagate through the matrix over distances $> 10^2$ – 10^3 Å (The electron escape length in a thick sample ($d > 0.02$ μm) of solid argon is expected to be > 2000 Å at 10 eV).²³ Since the cross section for electron-cation recombination is much larger than that for electron attachment to a neutral molecule, the probability for the free electron produced by the photoionization of a neutral naphthalene molecule to recombine with a naphthalene cation is greater than the probability to recombine with the other neutral molecules or electron acceptors in the matrix. Thus, at high concentration, apparently in the $M/R = 100$ –300 range, the photoelectron is more likely to be captured by $C_{10}H_8^+$ than $C_{10}H_8$ leading to a situation of no ion concentration buildup in the matrix. Conversely, at lower concentrations ($M/R \gtrsim 500$), the separation between two precursors is apparently large enough for the free electron to become attached to a neutral naphthalene (leading to the formation of an anion $C_{10}H_8^-$) or other electron acceptor (such as impurities) sitting in a distinct site in the matrix instead of neutralizing a cation. The net effect of such a process is an increase in the ionic content of the matrix at the beginning of the photolysis. Once a certain concentration is achieved however, a steady state is reached and further ion buildup is inhibited. This model, called the charge saturation model, is discussed in Refs. 6 and 9(c). This concentration behavior also suggests that neutral naphthalene is the major electron acceptor under our experimental conditions.

Influence of VUV photolysis duration: The effect of VUV irradiation time on the growth of the cation bands and correlated depletion of neutral naphthalene is shown in Figs. 7(a) and 7(b). It is clear from the general behavior of the curves that the ion concentration increases sharply during the first 10 minutes of photolysis. The ion formation rate then decreases and reaches a steady state after about 40 minutes. These results can again be interpreted using the charge saturation model.⁶ Initially, when only neutral naphthalene molecules are present in the matrix, the absorption of a VUV photon results in the ejection of an electron from the parent molecule producing $C_{10}H_8^+$. Each free electron loses its excess energy in collisions with the lattice atoms along its mean path in the matrix and eventually becomes attached to an acceptor forming a molecular anion. After the first period of irradiation, enough cations are formed in the matrix so that the probability for a free electron to recombine with and neutralize a positively charged ion instead of a neutral precursor increases substantially, leading again to a steady state situation where the destruction of a cation accompanies each creation of another cation. This process hinders the formation of more cations in the matrix inducing the observed leveling off in the cation production rate (Fig. 7).

Electron acceptor: The inclusion of an electron acceptor in the matrix material is a common technique^{9(b),(c)} used to counter the limitation on cation production described above. Instead of using the customary acceptors, which often in-

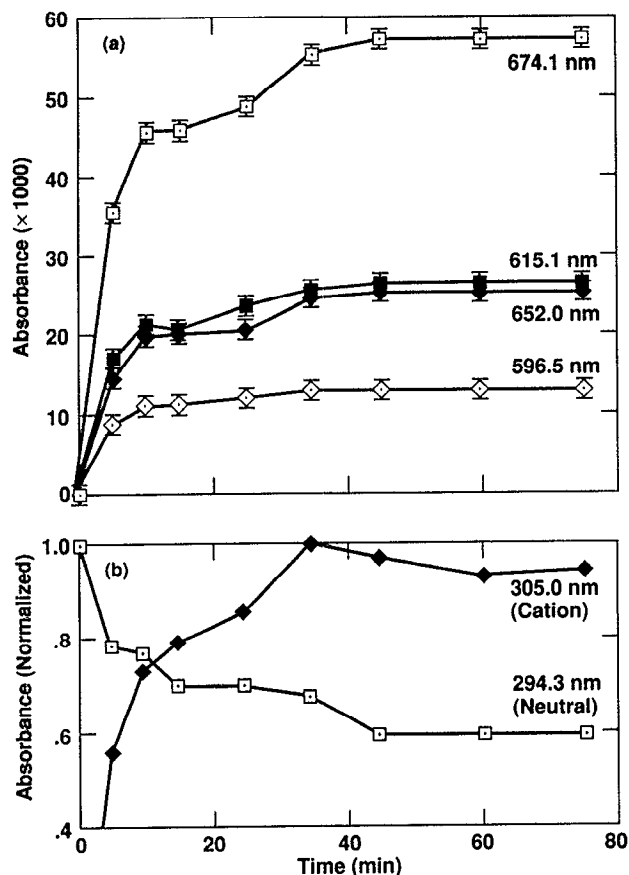


FIG. 7. (a) The growth of the visible naphthalene cation bands and (b) the normalized growth of the naphthalene cation 305.0 nm band and decrease of the neutral naphthalene 294.3 nm band as a function of VUV irradiation time. Naphthalene/Neon = 1/600, $T = 4.2$ K, 10 mmole h^{-1} deposition rate for 2.5 h.

involve halogens and might influence the photoproduct spectra sufficiently to hamper their application to astrophysical problems, we carried out several experiments using C_2H_2 . This molecule was chosen because the photofragment, C_2 , is known to have a strong electron affinity (3.39 eV), readily forming C_2^- .²⁴ The addition of C_2H_2 was, however, of only little practical benefit, leading to an increase of only about 10% in the cation yield (in experiments with starting concentrations of $Ar/C_{10}H_8/C_2H_2 = 600:1:1$ and $1000:1:2$) while adding complexity to the intermolecular interactions which occur in the solid and, hence, to the spectroscopic interpretation of the data. Surprisingly, while the $C_{10}H_8^+$ yield was not substantially increased, the C_2^- absorption band strengths were greatly enhanced. On the other hand, Andrews *et al.*^{9(b)} observed a threefold increase in the $C_{10}H_8^+$ production by the addition of strong electron traps (CCl_4) to their naphthalene in an argon matrix. The presence of this electron acceptor however, while slightly shifting the peak positions to the blue by $\sim 10 \text{ cm}^{-1}$ in the visible and $\sim 20 \text{ cm}^{-1}$ in the ultraviolet, may significantly enhance their transition strengths (see Sec. IV B).

Effect of photoexcitation energy: The effect of the photon energy of the VUV source on the ionization efficiency was examined by comparing the cation yields resulting from the

irradiation of the matrix-isolated naphthalene with two different spectral distributions. In the first case, the hydrogen lamp spectrum consisted of a strong 20 nm broad band centered at 160 nm and a weaker 121.6 nm atomic line (3.0×10^{-2} T of flowing pure H_2). In the second case, the radiation consisted of quasimonochromatic 121.6 nm Lyman α (3.0×10^{-2} T of a flowing H_2/He , 10% mixture). The cation yield increased by about 30% (measured with the 675.0 nm absorption band) in the second case. This is consistent with the fact that the 7.75 eV (160 nm) peak in the continuum of the pure hydrogen lamp falls below the first ionization potential of naphthalene—8.15 eV (152 nm)^{11(e),25}—and therefore does not contribute to the ionization process. This result also indicates that the electron solvation scheme, proposed by Brus and Bondybey^{24(b)} to account for the production of C_2^- by the ionization of C_2H_2 in matrices with photons of energy lower than the ionization potential for acetylene, does not play an important role in naphthalene ion production; and that the 0.7 eV red shift of the ionization potential of naphthalene in an argon matrix to 7.45 eV predicted by Kelsall *et al.*,^{9(c)} by analogy with the case of benzene,²⁶ must be readjusted to an upper limit of about 0.35 eV leading to a lower limit of 7.80 eV for the ionization potential. To check this, the experiment was repeated using the sapphire substrate as a filter to cut off radiation below 142.5 nm (8.70 eV). In this case, no ion bands were detected.

Effect of temperature: No temperature effects over the 5–35 K range were found. Annealing the naphthalene in an argon matrix ($M/R = 300, 600, 800, 1000,$ and 2000) at various temperatures from 4.2 K up to 20 K, before and after photolysis, had no effect on the ion yield. Similarly, holding the sample at 20 K after VUV irradiation at 4.2 K or holding the sample at 20 K during VUV photolysis had no effect on the cation concentration.

Deposition conditions: Cation yield was found to be independent of whether photolysis was carried out simultaneously with, or subsequent to, deposition. It was also independent of condensation rates over the range $2.5\text{--}10 \text{ mmole h}^{-1}$.

Photodetachment: Cation yield was found to be independent of the duration of exposure of the sample to the background radiation (180–900 nm) used for the spectral scan. This was verified, at various times, by taking a second scan right after the first one was completed.

IV. DISCUSSION AND SPECTROSCOPIC ASSIGNMENTS

A. Naphthalene

The absorption spectrum of neutral naphthalene has been studied extensively in the ultraviolet and visible regions of the optical spectrum and the spectroscopy of this molecule is well documented for the gas,^{16,19,25(a),27} liquid²⁸ and solid—pure crystal²⁹ and argon, krypton, and xenon-matrix isolated³⁰—phases. This is, to the best of our knowledge, the first report of the ultraviolet to near infrared absorption spectrum of naphthalene embedded in a neon matrix.

Naphthalene ($C_{10}H_8$) is a planar, alternating hydrocarbon which belongs to the D_{2h} symmetry group.³¹ Naphtha-

lene has 10 π electrons which produce the low energy singlet-singlet transitions (type $\pi-\pi^*$) in the ultraviolet. Figures 2(a) and 2(b) show the first three transitions from the ground (S_0) to the excited singlet states S_1 , S_2 , and S_3 with the possible contribution of a fourth, nontotally resolved, transition to S_4 at the high energy end of the spectrum. Some confusion exists in the literature regarding the assignments of all of these excited states. This is probably because the symmetry, and consequently the assignment, of the molecular states is a function of the labeling of the molecular axes. In this paper, we have chosen the configuration shown in Fig. 5, where the z axis is perpendicular to the plane of the molecule, the x axis corresponds to the long axis of the molecule (C_2 symmetry axis which bisects the edge C-C bonds), and the y axis is associated with the short axis of the molecule (C_2 symmetry axis passing through the central C atoms).

According to this convention, and by comparison with the well-known energy transitions occurring in naphthalene,^{27,28(a)} we assign the three vibronic systems observed in the spectrum of neutral naphthalene (Table I), in order of increasing energy, to the electronic transitions: ${}^1B_{3u}(S_1) \leftarrow X^1A_g(S_0)$, polarized along the long axis; ${}^1B_{2u}(S_2) \leftarrow X^1A_g(S_0)$, polarized along the short axis; and ${}^1B_{3u}(S_3) \leftarrow X^1A_g(S_0)$, polarized along the long axis. Furthermore, following the gas phase observations of George and Morris¹⁶ and the solid matrix (Ar, Kr, and Xe) measurements of Ref. 30(a), we tentatively assign the highest energy bands in the spectrum of naphthalene to a progression originating at 207.2 nm in an argon matrix (203.7 nm in neon) and associated to the forbidden transition ${}^1A_g(S_4) \leftarrow X^1A_g(S_0)$. While a detailed discussion of the vibrational assignments of the bands is beyond the scope of this work, a repeating pattern can be recognized in the energy intervals reported in Table I and when these are compared to the high resolution spectroscopic data available in the literature,^{19,30(b)} one can make reasonable vibrational assignments. These tentative assignments are listed in Table II for each absorption system in the two rare gas matrices examined (Ne and Ar). Moreover, the similarities—within the accuracy of the measurements—in the vibrational frequencies of the modes in the S_1 , S_2 , S_3 , and S_4 excited singlet states indicate that the geometry of the molecule is only slightly modified in the different electronic states. The data in Table II also show that, contrary to the red shift observed in the electronic band origins when going from neon to argon matrices (0.5% to 2.0%, see Table I and Sec. III A), the vibrational frequencies (intervals) remain unchanged ($\Delta\nu_{Ar-Ne}$ are less than the uncertainty of 20 cm^{-1}) when the matrix material is changed. Considering, now, the frequencies of the well-known vibrational modes of the ground state S_0 ,³² and assuming that the geometry of the molecule changes only slightly, one is tempted to draw a rough parallel between the frequencies and these fundamental vibrations. In this spirit, we tentatively attribute the two lowest energy modes [$\nu_8(b_{1g})$ and $\nu_9(a_g)$] to the skeletal motions of the molecule (out-of-plane bending), the third [$\nu_8(a_g)$], which usually only appears in combination with CC motions, to a C-H out-of-plane bending mode, the fourth

[$\nu_7(b_{1g})$] either to an in-plane C-H bend or the combination of the first two skeletal modes, and the highest energy vibration [$\nu_4(a_g)$] to the vibration of the bond common to both rings. The $\nu_5(b_{1g})$ and $\nu_4(b_{1g})$ modes are more difficult to attribute, but may correspond to an in-plane C-H bend and a C-C stretch, respectively.

B. Naphthalene cation

Assignments of the vibronic band systems produced by vacuum ultraviolet irradiation of naphthalene isolated in argon and neon matrices which are associated with the molecular cation $C_{10}H_8^+$ are given in Table III. These assignments can only be taken as tentative in the absence of corroborative calculations of the cation's molecular orbitals (MO) which take into account the contribution of all the electrons of the system. A semiempirical approach is, however, possible using the Hückel Molecular Orbital (HMO) theory³³ to calculate the energy of the π orbitals of the system.^{11(c)} The 10 π molecular orbital energy level diagram of naphthalene, calculated^{9(b),10(a)} using the value of 2.77 eV for the resonance integral β deduced from PES measurements,^{11(a)} is shown in Fig. 5 together with the electron distribution corresponding to the ground state cation. The molecular orbitals are denoted following the alphabetical terminology introduced by Shida and Iwata^{7(b)} and the symmetry of each species—in the D_{2h} symmetry group representation—are also indicated. Considering the *one-electron* excitation schemes possible from the cation ground state configuration $\{(b_{1u})^2(b_{2g})^2(b_{3g})^2(b_{1u})^2(a_u)^1\}$ which corresponds to the doublet state $X^2A_u(D_0)$ leads to a variety of excited doublet and quadruplet states (${}^{2S+1}D_j, S = 1/2, 3/2; j > 0$). Taking into account the parity and spin selection rules regulating such transitions, one can *tentatively* assign most of the observed cation absorption features—in order of increasing energy—(Figs. 3 and 4) as follows:

- (i) The visible absorption system originating around $14\,800\text{ cm}^{-1}$ in both Ne and Ar matrices (see Table III) is assigned to the $d \rightarrow f$ long-axis polarized excitation ($15\,321\text{ cm}^{-1}$ calculated) which corresponds to the ${}^2B_{3g}(D_2) \leftarrow X^2A_u(D_0)$ transition. [The $e \rightarrow f$ transition into the first excited doublet state (${}^2B_{1u}(D_1)$, predicted by the HMO theory at about 8550 cm^{-1} , is symmetry forbidden.]
- (ii) The absorption band which appears around $21\,930\text{ cm}^{-1}$ in a Ne matrix is assigned to the $c \rightarrow f$ short-axis polarized excitation ($22\,340\text{ cm}^{-1}$ calculated) and corresponds to the ${}^2B_{2g}(D_3) \leftarrow X^2A_u(D_0)$ transition.
- (iii) The ultraviolet absorption at $26\,530\text{ cm}^{-1}$ in Ne matrices ($26\,330\text{ cm}^{-1}$ in Ar) is assigned to the $f \rightarrow g$ short-axis polarized excitation ($27\,580\text{ cm}^{-1}$ calculated) corresponding to the ${}^2B_{2g}(D_4) \leftarrow X^2A_u(D_0)$ transition.
- (iv) The $f \rightarrow h$ and $e \rightarrow g$ long-axis polarized excitations are degenerate with a calculated energy of $36\,125\text{ cm}^{-1}$, close to the observed $36\,232\text{ cm}^{-1}$ (Ne matrix) and $36\,430\text{ cm}^{-1}$ (Ar matrix) absorptions (Table III). These excitations are associated with a ${}^2B_{3g} \leftarrow X^2A_u(D_0)$ transition.
- (v) The highest measured energy transition falls around $45\,000\text{ cm}^{-1}$ in Ne ($45\,600$ in Ar) and may be assigned to the $e \rightarrow h$ short-axis polarized excitation ($44\,670\text{ cm}^{-1}$ cal-

culated) and corresponds to a ${}^2B_{2g} \leftarrow X^2A_u(D_0)$ transition.

It is worthwhile to repeat that these assignments are only tentative until more elaborate calculations are performed to explore the precise nature of each transition. Moreover, two ultraviolet absorptions cannot be assigned by the HMO approach, namely the band system originating around $32\,400\text{ cm}^{-1}$ (Ne) and the weak band measured at about $41\,000\text{ cm}^{-1}$ (Ne). It is tempting, however, following Andrews *et al.*^{9(b)} to assign the $32\,400\text{ cm}^{-1}$ progression to the analog of the energetically similar $32\,100\text{ cm}^{-1}$ transition in the neutral molecule (System I in Table I). Such an analogy would correspond to a ${}^2B_{3g} \leftarrow X^2A_u(D_0)$ type of assignment for this transition.

Three repeating fundamental energy intervals can be clearly recognized in the lowest energy absorption system of the cation at 502 , 849 , and 1423 cm^{-1} in Ne. These vibrational frequencies remain unchanged when going from a neon to an argon matrix (see Table III). The assignment of these frequencies can be proposed by comparison with the literature. The absorption spectrum of $C_{10}H_8^+$, formed by γ irradiation of the neutral molecule in a Freon glass,¹² shows three similar fundamentals at 510 , 895 , and 1428 cm^{-1} as well as their overtones and combinations, while the resonance Raman spectrum shows two intense fundamentals at 511 and 1398 cm^{-1} as well as a weak band at 769 cm^{-1} . The argon matrix data of $C_{10}H_8^+$ [Ref. 9(b)] indicate vibrational intervals of 504 , 754 , and 1422 cm^{-1} as well as a weaker band at 846 cm^{-1} , which are assigned by comparison with the fully deuterated counterpart absorptions. Moreover, by analogy with the case of the neutral molecule (see Sec. IV A above and Table II), and considering that the geometry of the cation in its lower excited states should be quite similar to that of the neutral molecule, one can tentatively assign the cation vibrational intervals. The 502 cm^{-1} component is thus associated with the $\nu_3(a_g)$ mode which arises from the out-of-plane skeletal distortion of the molecular cation. The 1423 cm^{-1} vibrational fundamental is related to the $\nu_4(a_g)$

mode which corresponds to the C–C stretching vibration of the bond common to both rings and the 849 cm^{-1} fundamental to the out-of-plane C–H bending mode. These assignments take into account the intensities of the resonance Raman spectra, with scattering involving unsaturated C–C bond vibrations expected to be much more intense than scattering involving C–H fundamentals. In the absence of detailed experimental and theoretical studies of the vibrational modes of $C_{10}H_8^+$ in the higher excited states, it is unwarranted to speculate on their vibrational assignments.

1. Molar absorption coefficients

The molar absorption coefficients listed in Table V for the naphthalene cation in neon and argon matrices were determined as follows. The number of neutral naphthalene molecules depleted as a function of irradiation time was obtained from the relation $N = \Delta\tau/\epsilon$. The absorbance τ ($-\log_{10} I/I_0$), both before and after photolysis, was determined directly from the measured spectra, and the peak molar absorption coefficient, ϵ , was taken from Ref. 16. A gas-phase ϵ value of $210\text{ dm}^3\text{ mol}^{-1}\text{ cm}^{-1}$ was used for the 309.2 nm (Ar) and the 307.6 nm (Ne) neutral naphthalene bands. System I was used as a reference point, because it is the only unsaturated neutral band system under the conditions required to yield satisfactory ion spectra (see Sec. III). In the calculations, scaled values of the 295.8 nm (Ar) and 294.3 nm (Ne) bands of system I were chosen in order to minimize uncertainties associated with cation band overlap. Assuming now that for each naphthalene cation formed, a naphthalene anion is simultaneously formed (since we have not introduced any electron acceptor in the matrix), implies that two neutral naphthalene molecules are depleted to form one cation. The peak molar absorption coefficients listed in Table V were then determined taking this into account. These values, accurate to within 20%, represent an average of the values measured during cation growth before reaching steady state (Fig. 7). Note that the absorption coefficients

TABLE V. Naphthalene cation vibronic transition band widths, absorption coefficients, oscillator strengths, and cross sections.

$\lambda(\text{nm})$	$\nu(\text{cm}^{-1})$	$\Delta\nu(\text{cm}^{-1})$	ϵ_{max}^+ ($1\text{ mol}^{-1}\text{cm}^{-1}$)	f^a	σ_e ($\text{cm}^2\text{ molec}^{-1}$)
Neon:					
674.1	14 835	120	900	0.000 40	3.4×10^{-18}
652.0	15 337	100	400	0.000 10	1.5×10^{-18}
615.1	16 258	100	410	0.000 10	1.6×10^{-18}
596.5	16 765	80	200	0.000 05	7.6×10^{-19}
				($\Sigma = 0.000\ 65$)	
456.0	21 930	140	43	0.000 02	1.6×10^{-19}
376.9	26 532	400	100	0.000 10	3.8×10^{-19}
305.0	32 787	215	1040	0.000 80	4.4×10^{-18}
Argon:					
675.0	14 815	75	1130	0.000 30	4.3×10^{-18}
652.7	15 322	65	572	0.000 13	2.2×10^{-18}
615.8	16 238	65	538	0.000 13	2.1×10^{-18}
597.4	16 739	80	292	0.000 08	1.12×10^{-18}
				($\Sigma = 0.000\ 64$)	

^a Calculated from [$nf = 4.32 \times 10^{-9} \epsilon_{\text{max}}^+ \Delta\nu$] (Ref. 34); $n(\text{Ne}) = 1.28$; $n(\text{Ar}) = 1.29$ (Ref. 35).

reported here are significantly lower (by a factor of 25) than those reported by Kelsall and Andrews^{9(c)} in argon matrices, but are within a factor of 3, 5, and 6 to those measured in polar solutions and matrices.^{8(a),(b),7(d)} These discrepancies may be due to the enhancement of the oscillator strength by the CCl_4 used by Kelsall and Andrews as an electron acceptor and/or by the high polarizability of the solutions used in Refs. 8(a) and 8(b) and 7(d). Moreover, our measurements in neon and argon matrices (Table V) indicate that ϵ^+ increases with the degree of polarizability of the matrix. The values in neon are close (within a factor of 2) to the corresponding values for the neon-matrix isolated coronene cation.³⁶

V. CONCLUSIONS

The ultraviolet to near infrared (180–900 nm) absorption spectra of naphthalene ($C_{10}H_8$) and its radical cation ($C_{10}H_8^+$), formed by direct vacuum-ultraviolet photoionization, have been studied in neon and argon matrices. This study in solid Ne provides the first information on the spectroscopy of these molecular species *when (largely) unperturbed by the medium*, a condition which is crucial for astro-physical applications.

Four ultraviolet absorption systems, having similar vibrational frequencies, are reported for the neutral molecule. The absorption spectrum of the radical cation isolated in solid Ne shows seven progressions in the visible and the ultraviolet regions. Only five were detectable in Ar matrices. The measurements are in agreement with the photoelectron spectra of naphthalene, the absorption and photodissociation spectra of naphthalene cations, and the predictions of semiempirical HMO calculations. Taken together, these similarities permit one to assign the lower energy electronic transitions of the cation. These results also show the need for more sophisticated calculations to help in the assignment of the two highest energy transitions, reported here for the first time, in the absorption spectrum of the radical cation. These data, and similar studies on larger PAHs are critically needed to interpret observations of the interstellar medium.

Note added in proof. We have examined the effects induced on the formation yield of $C_{10}H_8^+$ by the addition of CCl_4 as an electron acceptor to the matrix. Single photon ionization of $C_{10}H_8/CCl_4/Ar$ and $C_{10}H_8/CCl_4/Ne$ matrices with 10.2 eV photons mainly produces CCl_4^+ at the expense of $C_{10}H_8^+$. Two-photon ionization of a $C_{10}H_8/CCl_4/Ar$ matrix with 4.9 eV photons results in a strong enhancement of the $C_{10}H_8^+$ bands, in agreement with the results of Ref. 9(b). *However*, in the case of a $C_{10}H_8/CCl_4/Ne$ matrix, 4.9 eV *do not form* naphthalene cations. A discussion of these results and their implications is presented in a forthcoming article.³⁸

ACKNOWLEDGMENTS

The authors want to thank R. Walker for his invaluable expert assistance in developing the experimental apparatus. The authors also want to express their gratitude to P. Du and G. Loew for communicating the results of their INDO/S-CI calculations on $C_{10}H_8^+$ prior to publication and to sincerely

acknowledge the very useful comments of S. Leach throughout this work. This work was done while F. S. held a National Research Council-NASA/Ames Research Center Associateship. This project was supported by NASA Grant No. 188-44-57-01.

- ¹ (a) L. J. Allamandola, A. G. G. M. Tielens, and J. R. Barker, *Astrophys. J. Supp. Ser.* **71**, 733 (1989); (b) L. J. Allamandola, in *Topics in Current Chemistry*, edited by S. Cyvin and J. Gutman (Springer-Verlag, Berlin, 1990), p. 1.
- ² J. L. Puget and A. Léger, *Ann. Rev. Astron. Astrophys.* **27**, 161 (1989).
- ³ (a) G. P. Van der Zwet and L. J. Allamandola, *Astron. Astrophys.* **146**, 76 (1985); (b) A. Léger and L. B. d'Hendecourt, *ibid.* **146**, 81 (1985); (c) M. K. Crawford, A. G. G. M. Tielens, and L. J. Allamandola, *Astrophys. J. (Lett.)* **293**, L45 (1985).
- ⁴ B. Meyer, *Low Temperature Spectroscopy* (Elsevier, New York, 1971).
- ⁵ H. E. Hallam, in *Vibrational Spectroscopy of Trapped Species*, edited by H. E. Hallam (Wiley, New York, 1973), p. 11.
- ⁶ V. E. Bondybey and T. A. Miller, in *Molecular Ions: Spectroscopy, Structure and Chemistry*, edited by T. A. Miller and V. E. Bondybey (North-Holland, New York, 1983), p. 125.
- ⁷ (a) T. Shida and W. H. Hamill, *J. Chem. Phys.* **44**, 2375 (1966); (b) T. Shida and S. Iwata, *J. Am. Chem. Soc.* **95**, 3473 (1973); (c) A. Kira, M. Imamura, and T. Shida, *J. Phys. Chem.* **80**, 1445 (1976); (d) A. Kira, T. Nakamura, and M. Imamura, *ibid.* **81**, 511 (1977).
- ⁸ (a) R. Gschwind and E. Haselbach, *Helv. Chim. Acta* **62**, 941 (1979); (b) M. O. Delcourt and M. J. Rossi, *J. Phys. Chem.* **86**, 3233 (1982).
- ⁹ (a) L. Andrews and T. A. Blankenship, *J. Am. Chem. Soc.* **103**, 5977 (1981); (b) L. Andrews, B. J. Kelsall, and T. A. Blankenship, *J. Phys. Chem.* **86**, 2916 (1982); (c) B. J. Kelsall and L. Andrews, *J. Chem. Phys.* **76**, 5005 (1982); (d) J. Hacaloglu and L. Andrews, *Chem. Phys. Lett.* **160**, 274 (1989).
- ¹⁰ (a) R. C. Dunbar and R. Klein, *J. Am. Chem. Soc.* **98**, 7994 (1976); (b) M. S. Kim and R. C. Dunbar, *J. Chem. Phys.* **72**, 4405 (1980); (c) J. A. Syage and J. E. Wessel, *ibid.* **87**, 6207 (1987).
- ¹¹ (a) J. H. D. Eland and C. J. Danby, *Z. Naturforsch.* **23a**, 355 (1968); (b) M. J. S. Dewar and S. D. Worley, *J. Chem. Phys.* **51**, 263 (1969); (c) P. A. Clark, F. Brogli, and E. Heilbronner, *Helv. Chim. Acta* **55**, 1415 (1972); (d) E. Heilbronner, T. Hoshi, J. L. von Rosenberg, and K. Hafner, *Nouv. J. Chimie* **1**, 105 (1976); (e) E. Rühl, S. D. Price, and S. Leach, *J. Phys. Chem.* **93**, 6312 (1989).
- ¹² S. J. Sheng and G. Hug, *Chem. Phys. Lett.* **57**, 168 (1978).
- ¹³ (a) P. Warneck, *Appl. Opt.* **1**, 721 (1962); (b) J. A. Samson, in *Techniques of VUV Spectroscopy* (Wiley, New York, 1967), p. 137; (c) *ibid.* p. 160; (d) H. Okabe, *J. Opt. Soc. Am.* **54**, 478 (1964).
- ¹⁴ F. Salama (in preparation).
- ¹⁵ R. C. Weast and S. M. Selby, in *Handbook of Chemistry and Physics*, 69th ed. (Chem. Rubber Co., Cleveland, 1989).
- ¹⁶ G. A. George and G. C. Morris, *J. Mol. Spectrosc.* **26**, 67 (1968).
- ¹⁷ (a) R. W. B. Pearse and A. G. Gaydon, in *The Identification of Molecular Spectra* (Chapman & Hall, London, 1965), p. 239; (b) B. Coquart, M. F. Merienne, and A. Jenouvrier, *Planet. Space Sci.* **38**, 287 (1990).
- ¹⁸ M. L. Klein and J. A. Venables, in *Rare Gas Solids*, Vol. I (Academic, London, 1976).
- ¹⁹ (a) S. M. Beck, D. E. Powers, J. B. Hopkins, and R. E. Smalley, *J. Chem. Phys.* **73**, 2019 (1980); (b) F. M. Behlen, D. B. McDonald, V. Sethuraman, and S. A. Rice, *J. Chem. Phys.* **75**, 5685 (1981).
- ²⁰ P. Du and G. Loew (private communication).
- ²¹ S. Oberland and W. Schmidt, *J. Am. Chem. Soc.* **97**, 6633 (1975).
- ²² (a) R. E. Behringer, *J. Chem. Phys.* **29**, 537 (1958); (b) E. Rytter and D. M. Gruen, *Spectrochim. Acta* **35A**, 199 (1979).
- ²³ Z. Ophir, B. Raz, J. Jortner, V. Saile, N. Schwentner, E. E. Koch, M. Skibowski, and W. Steinmann, *J. Chem. Phys.* **62**, 650 (1975).
- ²⁴ (a) P. L. Jones, R. D. Mead, B. E. Kohler, S. D. Rosner, and W. C. Lineberger, *J. Chem. Phys.* **73**, 4419 (1980); (b) L. E. Brus and V. E. Bondybey, *ibid.* **63**, 3123 (1975); (c) L. J. Allamandola, H. M. Rojhantalab, J. W. Nibler, and T. Chappell, *ibid.* **67**, 99 (1977).
- ²⁵ (a) E. E. Koch, *Chem. Phys. Lett.* **16**, 131 (1972); (b) M. A. Duncan, T. G. Dietz, and R. E. Smalley, *J. Chem. Phys.* **75**, 2118 (1981).
- ²⁶ A. Gedanken, B. Baz, and J. Jortner, *J. Chem. Phys.* **58**, 1178 (1973).
- ²⁷ M. B. Robin, in *Higher Excited States of Polyatomic Molecules* (Academic, New York, 1975), p. 257.

- ²⁸ (a) J. B. Birks, in *Photophysics of Aromatic Molecules* (Wiley, London, 1970), p. 70; (b) O. E. Weigang, *J. Chem. Phys.* **33**, 892 (1960); (c) H. B. Klevens and J. R. Platt, *ibid.* **17**, 470 (1949).
- ²⁹ (a) T. A. Krivenko, A. V. Leiderman, I. P. Terenetskaya, and E. F. Sheka, *Opt. Spectrosc. (USSR)* **45**, 16 (1978); (b) D. W. Schlosser and M. R. Philpott, *Chem. Phys.* **49**, 181 (1980).
- ³⁰ (a) S. S. Hasnain, P. Brint, and T. D. S. Hamilton, *J. Mol. Spectrosc.* **72**, 349 (1978); (b) M. Gutmann, P. F. Schonzart, and G. Hohlneicher, *Chem. Phys.* **140**, 107 (1990).
- ³¹ D. S. McClure, *J. Chem. Phys.* **24**, 1 (1956).
- ³² (a) E. R. Lippincott and E. J. O'Reilly, *J. Chem. Phys.* **23**, 238 (1955); (b) A. L. McClellan and G. C. Pimentel, *ibid.* **23**, 245 (1955).
- ³³ C. A. Coulson, *Proc. Phys. Soc.* **60**, 257 (1948).
- ³⁴ H. Okabe, in *Photochemistry of Small Molecules* (Wiley, New York, 1978), p. 41.
- ³⁵ H. Jodl, in *Chemistry and Physics of Matrix-Isolated Species*, edited by L. Andrews and M. Moskovits (North-Holland, New York, 1989), p. 343.
- ³⁶ P. Ehrenfreund (private communication).
- ³⁷ G. Herzberg, in *Infrared and Raman Spectra of Polyatomic Molecules* (Van Nostrand, New York, 1945).
- ³⁸ F. Salama and L. J. Allamandola (to be submitted for publication in *J. Chem. Phys.*).